NONTECHNICAL SUMMARY

Constraints on energy dissipation in the earth's body tide from satellite tracking and altimetry

The gravitational tug of the moon and sun generate tides in the ocean, the atmosphere, and the solid earth. The earth tides are typically about 30 cm. Because the earth is not perfectly elastic, there is a small lag in the earth's response to the tidal forcing. The lag is very small and difficult to determine, nearly hidden within the much larger response of the oceans. But knowledge of the lag tells us important information about the earth's deep interior.

We have recently determined the earth's tidal lag by combining radar data from the Topex/Poseidon altimeter with laser tracking data of Lageos-1 and several other satellites. The combination of geometrical measurements from Topex/Poseidon with (in essence) gravitational measurements from Lageos allows us to separate the tidal effects of oceans and solid earth. We find a phase lag in the earth's principal semidiurnal lunar tide of $0.204° \pm 0.047°$, corresponding to a time lag of approximately 25 seconds. This implies that the solid tide dissipates at least 110 gigawatts of tidal power, or about 5% of what the ocean tides dissipate.

R. Ray (926.)

submitted to *Geophys J Int*

Constraints on energy dissipation in the earth's body tide from satellite tracking and altimetry

Richard D. Ray[1], Richard J. Eanes[2] and Frank G. Lemoine[1]

[1] *Space Geodesy Branch, NASA Goddard Space Flight Center, Greenbelt, MD, USA*

[2] *Center for Space Research, University of Texas, Austin, TX, USA*

SUMMARY

The phase lag by which the earth's body tide follows the tidal potential is estimated for the principal lunar semidiurnal tide M_2. The estimate results from combining recent tidal solutions from satellite tracking data and from Topex/Poseidon satellite altimeter data. Each data type is sensitive to the body-tide lag: gravitationally for the tracking data, geometrically for the altimetry. Allowance is made for the lunar atmospheric tide. For the tidal potential Love number k_2 we obtain a lag ϵ of $0.20° \pm 0.05°$, implying an effective body-tide Q of 280 and body-tide energy dissipation of 110 ± 25 gigawatts.

Key words: tides – earth tides – ocean tides – Love number – Q

1 INTRODUCTION

Kelvin's famous dictum that the earth has the rigidity of steel arose from consideration of the tides. Over the next hundred years developments in seismology greatly refined our picture of the earth's interior, rightly overshadowing any small contribution from tidal studies. Yet knowledge of the earth's anelastic dispersion requires data outside the relatively narrow seismic band. At periods between 10 hours and 20 years, the tides and the closely related nutations are very nearly the only tools in hand.

It is therefore understandable that much excitment was generated in the mid-1960's when tidal perturbations were first detected in the orbits of artificial satellites These perturbations appeared to be a direct route to determining the global earth tide, and several groups (e g , Newton 1968; Kozai

1968; Smith, Kolenkiewicz & Dunn 1973) soon published estimates of the potential Love number k_2, including the small component out-of-phase with the tidal potential. A clearly evident goal was to obtain observational estimates of the angle $\epsilon = -\arg k_2$, defining how the solid tidal strain lags the tidal stress; from ϵ follow direct estimates of the body's specific dissipation function $Q^{-1} = \tan\epsilon$ and its tidal energy dissipation.

Unfortunately, none of these early attempts to deduce k_2 from satellite tracking data was successful. The estimates, particularly those of ϵ, were corrupted by the ocean tide, which gives rise to the same spectrum of orbit perturbations as the solid tide (Lambeck, Cazenave & Balmino 1974) yet was too poorly determined to remove from the data. By the mid-1970's this was generally acknowledged and attempts to infer ϵ from satellite data were largely abandoned. Over the next two decades the accepted procedure for analyzing satellite data was to adopt a prior model (usually an elastic model) of the body tide and to assume that all remaining tidal signals were due to the ocean tide (and its load deformation).

In light of the vastly improved knowledge of the tides from the Topex/Poseidon (hereinafter T/P) satellite altimeter mission (Le Provost, Bennett & Cartwright 1995), a clearer separation of ocean and earth tide signals in satellite data is now possible. In essence the separation is possible because the tracking data are sensitive to the gravitational effect of the ocean + earth tides, while the altimeter data are sensitive to the geometrical (elevation) effect. We recently published an attempt to extract ϵ from tracking and altimeter data, obtaining $\epsilon = 0.16°$ and $Q = 370$, although with rather large error limits (Ray, Eanes & Chao 1996). The present paper is a much more thorough discussion of the analysis of an expanded dataset. The newer data allow the uncertainties in ϵ and Q to be tightened considerably. As in the initial paper, attention is restricted to the principal lunar semidiurnal tide M_2; the solar tides are confounded by insolation and atmospheric effects, while the diurnal tides are smaller and less reliably determined

This work is based on estimates of the degree-2, order-2, prograde coefficients of M_2, which describe the nominal ocean tide as reported from altimetric and tracking analyses. (In this context, "prograde" means in the direction of the tide-raising body, i.e., westward.) In terms of its geometrical height fluctuation relative to the seabed, we express this wave as

$$\zeta(\theta,\varphi,t) = D_{22}^{+}\cos(\omega t + 2\varphi - \psi_{22}^{+})\,P_2^2(\cos\theta) \tag{1}$$

where (θ,φ) are spherical polar coordinates, ω is the frequency of M_2, and P_2^2 is an (unnormalized) associated Legendre function. Section 3 lays out the method whereby altimetric and tracking estimates of D_{22}^{+} and ψ_{22}^{+} may be combined to yield ϵ. This is followed by sections describing our adopted altimetric and tracking solutions Careful attention must be given to the tracking solutions to ensure consistency in adopted geophysical constants and mathematical formulations. (The altimeter

solutions are all based on various analyses of T/P data; they are already consistent in regard to adopted constants.) Section 7 presents our deduced estimates of the lagged body tide, followed by a discussion and comparison to other models and previous estimates.

2 HISTORICAL PERSPECTIVE

It is enlightening to consider the various attempts over the past several decades to deduce the tidal coefficients $(D_{22}^{+}, \psi_{22}^{+})$ from hydrodynamic models, from oceanographic data, and from satellite data. Figure 1 shows four historical snapshots of estimates for the years 1977, 1986, 1991, and 1995. Note the change in scale for each diagram; the zoomed square in Figures 1a, 1b, and 1c represents the whole of Figure 1d. The plotted data are not comprehensive—every published value over four decades could hardly be included—but we have attempted to include estimates that at these times were widely known and were considered serious attempts at accuracy. Some points (e.g., those of Schwiderski and Parke & Hendershott) are included in more than one diagram, because they continued to be widely employed over many years. Coefficients for some of the early models were not given by the original authors but were computed by Lambeck (1977) from the original cotidal charts, we have extracted the relevant data from Lambeck's tabulations. The overall picture from Figure 1 is surely one of considerable and steady progress.

Figure 1d (circa 1995) is adopted from Ray *et al.* (1996). It is the first in which accurate estimates from the T/P altimeter mission are included. The updated version of this diagram for the present paper is given in Figure 2, which shows tidal coefficients described below in Sections 4 and 5.

In both Figures 1d and 2 it is clear that the tracking and altimeter estimates form two separate clusters, with an approximately 4% discrepancy in the out-of-phase component. This discrepancy forms the basis of the present paper. Our interpretation of the discrepancy, following our earlier paper, is that it arises from the different ways an anelastic body tide perturbs altimetric and tracking estimates of the ocean tide when both adopt strictly elastic solid-tide models. The discrepancy allows a direct empirical determination of the anelastic component $k_2 \sin \epsilon$ of the body tide.

3 THEORY

The basic approach is to examine the secondary tidal potentials that are induced by the tidal deformations of the earth, ocean, and atmosphere. Satellite orbit perturbations, monitored by the tracking observations, directly sense the entire planetary tidal potential. By decomposing this potential into its solid and fluid components and using the altimetry to estimate (primarily) the ocean component, one arrives at an expression that can be solved for the body lag ϵ based on the out-of-phase discrepancy

seen in Figure 2. We also allow for the possibility of estimating a load tide lag ϵ' from any in-phase discrepancy, although clearly for our data in Figure 2 such discrepancy must be small; moreover the standard errors for ϵ' turn out to be so large this estimate is of little value. The present section develops this outline in detail.

In the following we will drop sub- and superscripts on $D_{22}^{+}, \psi_{22}^{+}$, but will add superscripts T or A to denote Tracking or Altimetry solutions, respectively. We also drop subscripts on Love and loading numbers k_2, k_2'. These numbers will be treated as real, and any phase lag will be expressed explicitly through a complex factor $e^{-i\epsilon}$.

Assume the earth is a spherical body of radius a. Errors caused by the neglect of the earth's flattening should amount to no more than 0.3%, which is an order of magnitude smaller than the 4% discrepancy that forms the basis of our analysis. Future work may merit rigourous accounting for the flattening, but the simplicity of the spherical approximation prompts us to ignore it for now.

The primary astronomical potential for M_2 on the earth's surface can then be written (Cartwright & Tayler 1971)

$$\Phi^P(\theta, \varphi, t) = g\bar{H}\, P_2^2(\cos\theta)\, \cos(\omega t + 2\varphi) \tag{2}$$

where g is the gravitational acceleration, ω is frequency, t is time reckoned from the instant the mean moon passes the Greenwich (or 180°) meridian, and $P_2^2(\cos\theta) = 3\sin^2\theta$. The constant $\bar{H}$ is an equilibrium tidal amplitude (potential divided by g) as given in the tables of Cartwright & Edden (1973):

$$\bar{H} = \sqrt{(5/96\pi)} \times 63.194\,\text{cm} = 8.1367\,\text{cm} \tag{3}$$

A secondary potential Φ^S is generated by the planetary tidal deformations. It can be decomposed into three components:

$$\Phi^S = \Phi_B^S + \Phi_{O+L}^S + \Phi_{A+L}^S, \tag{4}$$

arising from the body tide, the ocean tide and its load, and the atmospheric tide and its load.

Let us write all potentials in the form

$$\Phi(\theta, \varphi, t) = \text{Re}[\hat{\Phi}\, P_2^2(\cos\theta)\, e^{i(\omega t + 2\varphi)}] \tag{5}$$

where $\hat{\Phi}$ is a complex amplitude exclusive of P_2^2. Thus, the primary potential simplifies to $\hat{\Phi}^P = g\bar{H}$. Corresponding expressions for the secondary potentials are

$$\hat{\Phi}_B^S = g\bar{H}ke^{-i\epsilon} \tag{6}$$

$$\hat{\Phi}_{O+L}^S = (3\rho_w/5\rho_e)g(1 + k'e^{-i\epsilon'})De^{-i\psi} \tag{7}$$

$$\hat{\Phi}_{A+L}^S = (3/5\rho_e)(1 + k'e^{-i\epsilon'})Ee^{-i\chi} \tag{8}$$

where ρ_w is the mean density of seawater, ρ_e is the mean density of the earth, (D, ψ) are coefficients of the ocean tide (corresponding to the one prograde spherical harmonic given by Eq (1)), and (E, χ) are similar coefficients for the atmospheric tide (determined from barometric data) The expression for $\hat{\Phi}_B^S$ is simply the primary potential scaled by the k Love number and lagged by the angle ϵ. The expressions for ocean and atmospheric potentials are well-known thin-shell formulae (*e.g.*, Platzman 1984, Eq. 6) which allow for earth loading through the factor $(1 + k')$ but with k' also lagged by the angle ϵ'.

We must now relate these expressions to what the tracking and altimeter systems estimate for the nominal ocean tide. The tracking is most straightforward: in some sense it simply measures the total $\hat{\Phi}^S$ and then expresses it as an elastic body tide and a residual ocean tide (including its elastic load):

$$\hat{\Phi}^S = kg\bar{H} + \alpha g(1 + k')D^T e^{-i\psi^T} \tag{9}$$

where $\alpha = (3\rho_w/5\rho_e) = 0.1126$ (Complications caused by, for example, use of complex Love numbers in the tracking solutions will be dealt with in Section 5.)

Now the altimeter solutions are based on measurements of the geocentric tide, from which ocean tides are deduced by again adopting elastic body and load-tide models. That is, rather than directly evaluating $\zeta(\theta, \varphi, t)$ of (1) the altimeter solutions are actually evaluations of

$$\zeta + \Delta\zeta_b + \Delta\zeta_l$$

where $\Delta\zeta_b$ is the difference between the true lagged body tide and the adopted elastic model, and $\Delta\zeta_l$ the difference between the true load tide and its elastic model. Hence, for Love number h and load number h',

$$\begin{aligned} D^A e^{-i\psi^A} &= De^{-i\psi} + h\bar{H}(e^{-i\epsilon} - 1) \\ &\quad + De^{-i\psi}\alpha h'(e^{-i\epsilon'} - 1), \end{aligned} \tag{10}$$

(These expressions tacitly assume that the lag in the potential Love number k is identical to the lag in the displacement Love number h, and similarly for the load numbers k' and h' Strictly, this need not be so, although they are not expected to differ by large amounts. According to Zschau & Wang (1986) the lags in k and h differ by roughly 20%. In any event, the correction terms involving h and h' are small, and any errors in equating their lags to k and k', respectively, have little effect on our estimate of ϵ.)

We are now in position to equate the tracking and altimeter expressions for $\hat{\Phi}^S$—that is, Eqs. (9) and (4, 6–8,10)—on the assumption that the only unknown quantities are ϵ and ϵ'. In equating these expressions it is helpful to anticipate the smallness of ϵ and ϵ' by keeping only up to first order in these

quantities. After some algebraic manipulation, we arrive at

$$C_1\left(D^T e^{i\psi^T} - D^A e^{i\psi^A}\right) - C_3 E e^{i\chi} = (k - C_2)i\epsilon + \frac{k'}{1+k'} i\epsilon' \left(C_1 D^A e^{i\psi^A} + C_3 E e^{i\chi}\right) - \alpha h' i\epsilon' \left(C_1 D^T e^{i\psi^T} - C_3 E e^{i\chi}\right) \tag{11}$$

where

$$C_1 = \alpha(1+k')/\bar{H} = 0.9590\,\mathrm{m}^{-1} \tag{12}$$

$$C_2 = \alpha(1+k')h = 4.752 \times 10^{-2} \tag{13}$$

$$C_3 = \alpha(1+k')/(\rho_w g \bar{H}) = 9.445 \times 10^{-5}\,\mathrm{Pa}^{-1}. \tag{14}$$

By taking real and imaginary parts we arrive at two equations from which ϵ and ϵ' are found. The real part alone suffices to determine ϵ'.

The form of Eq. (11) shows clearly the role of the air tide: on the right-hand side the air tide terms are insignificant because they are in direct competition with the ocean tides; on the left-hand side, however, they may be important because they compete with the much smaller (altimeter − tracking) difference. It turns out (see below) that the air tide term on the left is marginally significant.

The term involving h' is roughly five times smaller than the term involving k'. In fact, the estimate of ϵ is overall rather insensitive to the ϵ' terms, and a fairly good approximate solution is obtained from simply the first terms on both the left and right of (11), giving

$$\epsilon \approx \frac{C_1}{k - C_2}\left(D^T \sin\psi^T - D^A \sin\psi^A\right). \tag{15}$$

4 SATELLITE ALTIMETER SOLUTIONS

The altimeter solutions adopted in this study and shown in Figure 1 are tabulated in Table 1. They are based on independent analyses of T/P altimeter data. Three of the four are second-generation solutions, relying on more than six years of data. All four solutions, or their precursors, were found by Shum *et al* (1997) to be among the more accurate T/P-based descriptions of the M_2 tide, based on comparison tests with deep-sea tide gauges and bottom pressure recorders and on variance reduction tests with independent altimeter data.

Both GOT99.2 and CSR4.0 result from empirical tidal analyses of the T/P data, using methods following Cartwright & Ray (1990) and/or Schrama & Ray (1994). The tidal solutions in both GOT99.2 and CSR4.0 represent long-wavelength adjustments to the hydrodynamic finite-element model FES94 1 of Le Provost *et al* (1994). The other two models in Table 1 are assimilation-type solutions. The TPXO.4 model is an update to that described by Egbert *et al.* (1994); its estimates of

tidal elevations (and currents) are the result of fitting to both linearized hydrodynamic equations and direct T/P sea-surface height observations. The FES95 2 model (Le Provost *et al.* 1998) assimilated the earlier CSR2.0 empirical solution into a finite-elelment hydrodynamic model, using methods fairly similar to those developed by Egbert *et al.* (1994).

All four T/P tidal solutions removed the body tide signal from the altimeter data by using an elastic model with Love number $h_2 = 0.609$, which is taken from Wahr (1981). The tidal potential employed was the harmonic development of Cartwright & Edden, updated to the 1990–2000 epoch (which is consistent with our value for $\bar{H}$ quoted above). Ocean loading corrections were applied based on high-degree spherical harmonic decompositions and the h'_n loading numbers of Farrell (1972); these calculations are typically performed in an iterative operation following Appendix A of Cartwright & Ray (1991).

The required M_2 coefficients (D, ψ) are computed by numerical quadrature of the various cotidal elevation charts. Accurate estimates, of course, require global data, yet the T/P observations are limited to the latitude band between 66°N and 66°S Hence, all solutions have been supplemented wherever necessary with numerical hydrodynamic tide models For both solutions CSR4.0 and GOT99.2, the FES94.1 hydrodynamic model of Le Provost *et al* (1994) was employed in all latitudes above 66°. The TPXO.4 solution used its own assimilation procedures in most of the polar regions and required supplemental data from FES94.1 only for the small Arctic region north of 80°N. While FES94.1 is probably one of the best tidal models available in polar seas, it cannot match the accuracy attained in regions where we have direct T/P measurements. Fortunately, the required (2, 2) spherical harmonic is fairly insensitive to the tide in the polar seas. For example, the contribution of FES94.1 to estimates of $D \sin\psi$ amounts to only 0.088 mm for the entire region north of 66°N (the region south of 66°S is just slightly larger), and presumably any error in FES94.1 would perturb the estimate far less than this. (Strictly, the use of hydrodynamic models to supplement the altimeter solutions is inconsistent with the analysis of the Section 3, which assumed global altimetry and allowed for an adjustment of the solid body and load tides. However, all hydrodynamic models account for very minor adjustments to the $D \sin\psi$ term, so any inconsistency in mixing altimeter and hydrodynamic models is of no great importance.)

The only reliable error analysis for the altimeter solutions is supplied with the TPXO 4 estimate of Egbert (personal communication, 1999). It is based on the inverse methods and error covariances described in Egbert *et al.* (1994), which are used in conjunction with some extensive Monte Carlo calculations similar to those described in Appendix A of Dushaw *et al.* (1997)

Some corroboration of the size of Egbert's error bar may be obtained by examining the global frequency-wavenumber spectra of ocean variability obtained by Wunsch & Stammer (1995) from their

analysis of T/P data. Their three-dimensional spectrum (see their Figure 2a) displays a tidal "ridge" at the period of 60 days (the tidal alias period in T/P) which is caused by M_2 (and also S_2) tide-model errors; the size of this ridge relative to the background spectrum might be taken as an indication of the size of the tide model error. (The published diagram was based on tide model CSR2.0; Wunsch (personal comm., March 1996) subsequently updated to model CSR3.0 and decomposed the spectra into eastward and westward propagating waves.) The power in the westward degree-2 wave is 0.04 cm^2. This includes all orders $m = -2, \ldots, 2$, and so may be divided by 5 for the $(2,2)$ term alone (although evidence suggests that the degree-2 zonal has much larger error than the degree-2 sectorial), giving an rms of 0.09 cm. This must be scaled by $\sqrt{(5/96\pi)}$ to account for the (lack of) normalization in (1), giving 0.011 cm for the combined tidal error plus oceanic variability. This suggests that the error quoted in Table 1—0.013 cm—is realistic, perhaps even conservative. It is roughly consistent with the scatter (standard deviation 0 016 cm) seen in Figure 2.

As our adopted altimeter solution we take the mean of the four models. Thus, for the out-of-phase component,

$$D^A \sin\psi^A = 3.219 \sin 129.814^\circ = 2.472 \pm 0.015\,\mathrm{cm}. \tag{16}$$

The standard error is Egbert's for TPXO.4 alone, but inflated to allow for the possibility of a roughly 0 3% systematic error from the neglect of earth ellipticity.

5 SATELLITE TRACKING SOLUTIONS

Six relatively recent tracking solutions for the M_2 coefficients (D, ψ) are collected in Table 2. They represent a variety of different approaches to analyzing satellite orbit perturbations and are based on a multitude of different satellite targets. Some solutions are parts of comprehensive inversions for the earth's static and time-variable gravity field using extensive historical and recent tracking data from many satellites; others are based on analysis of orbital residuals observed on one or a few satellites

We briefly describe each of these tidal solutions. GEM-T3S, EGM-96S, and GRIM5-S1 are comprehensive geopotential solutions, based on tracking data from 31, 40, and 21 satellites, respectively. The GRIM-5 solution is an update to that described by Schwintzer *et al.* (1997), tide coefficients and relevant constants were obtained courtesy of R. Biancale (personal comm , December 1999). The solution by Cheng (personal comm., July 1997), deduced from tracking observations of 8 geodetic satellites equiped with laser retroflectors, was part of a detailed study of temporal gravity variations (Cheng, Shum & Tapley 1997).

Somewhat more detail should be given for solutions LLA96-1 and -2, because they have not been described elsewhere. They are single-satellite solutions. LLA96-1 is based on approximately 20 years

of laser ranging to the geodetic satellite Lageos-1, LLA96-2 on slightly more than 3 years ranging to Lageos-2. For these solutions the most important data are measurements of long-period tidal perturbations in the satellite's inclination and node, for these are caused primarily by even-degree prograde harmonics of the tide. Data from a single satellite thus suffice to determine the coefficients D_{22}^+, ψ_{22}^+ and D_{42}^+, ψ_{42}^+. (Coefficients of degree 6 and above are less important for Lageos owing to its high altitude; they are adequately handled by a "background" prior tide model, in this case CSR3.0) Because the Lageos-2 time series is relatively short, the LLA96-2 standard error in Table 2 is understandably somewhat large While the Lageos-1 time series is much longer, its early data are relatively poor by modern standards. They have been considerably downweighted in the LLA96-1 solution, so its standard error is only 25% smaller than LLA96-2. A potential source of systematic error can arise from the proximity of the M_2 perturbation period (approximately 14 days for both Lageos satellites) to the large fortnightly variations in Earth rotation. If the rotation variations are mismodeled, they will directly corrupt tidal signals in the satellite's node and/or inclination, providing yet another reason to downweight the early Lageos-1 data.

The only other recent tracking solution that we are aware of is that published by Harwood & Swinerd (1997). They estimated $D_{22}^+ \sin\psi_{22}^+ = 3.11 \sin 132.0° = 2\ 31\ \text{cm} \pm 0.06\ \text{cm}$. This solution falls outside the borders of Figure 2 (notwithstanding its large error bar). It must be corrupted by some large systematic error(s), and it cannot be considered accurate.

5.1 Adjustment of tracking solutions

Part of the difficulty in using the tracking solutions of Table 2 is understanding and accounting for the variety of different geophysical constants and mathematical formulations used by the various orbit groups. Proper accounting for this is crucial. For this work it necessitated careful examination of the Goddard (GEODYN), Texas (UTOPIA), and French-German (GINS on the French side) computer codes and other documentations.

We begin with the mathematical formulation of the ocean tide potential. For the partial tide corresponding to the (2, 2) prograde component of M_2, as in Eq. (1), this potential is often written (e.g , Christodoulidis *et al.* 1988)

$$U(r,\theta,\varphi,t) = 4\pi G R_1 \rho_w \left(\frac{1+k_2'}{5}\right)\left(\frac{R_2}{r}\right)^3 \cdot \zeta(\theta,\varphi,t) \tag{17}$$

where G is the gravitational constant and r is the satellite radial distance The two distance scales in (17), R_1 and R_2, we discuss presently. The constants ρ_w, k_2, k_2' employed in the various tracking solutions are tabulated in Table 2.

Because we are essentially combining gravitational potential measurements with geometrical el-

evation measurements, we wish to ensure that the form of the potential U is as physically consistent as possible with the geometry of an ocean tide on the earth's surface (here assumed spherical as discussed in Section 3). The most problematic constant in this regard appears to be ρ_w. In accordance with Gill (1982) we take $\rho_w = 1035\ \mathrm{kg\,m^{-3}}$ as fairly representative of the mean density of the ocean. Most solutions adopt $\rho_w = 1025\ \mathrm{kg\,m^{-3}}$, which is more representative of the density of surface water. The density difference of 1% is significant, given that the fundamental discrepancy seen in Figure 2 is about 4%.

The "correct" values of the constants k_2 and k_2' are less clearcut. The 1996 conventions of the International Earth Rotation Service (McCarthy 1996, p.43) suggest an elastic value for k_2 of 0.29801 but an anelastic value of $0.30102 - i0.00130$ (which was adopted by Schwintzer *et al.* 1999). Other published values appear to vary by roughly ± 0.004. For consistency with the altimeter solutions and five of the six tracking solutions, we adopt the k_2 Love number of Wahr (1981): 0.302. By the Saito-Molodensky relationship, this and $h_2 = 0.609$ implies $k_2' = -0.307$. Some other published (real) values for k_2' are: -0.3075 (Farrell 1972), -0.3035 (Zschau 1978), -0.310 (Lambeck 1988), -0.309 (Pagiatakis 1990), -0.303 (Han & Wahr 1995). The scatter suggests that the error in our adopted k_2' is unlikely to exceed 1%. From (17) a 1% error in k_2' induces an error in D_{22}^{+} of about 0.4%. Errors in k_2 affect the out-of-phase component $D \sin\psi$ hardly at all. They do, however, induce potentially large errors in the in-phase component, which is relevant for ϵ' (see below).

The radii factors R_1, R_2 in (17) are somewhat murky (partly owing to our insistence on using a spherical earth). Fortunately, they are also less crucial. We take $R_1 = R_2 = a$, the mean radius of the earth, as being the most physically consistent radius to describe the tidally varying mass distribution. Christodoulidis *et al.* (1988, p. 6217 and 6230) write that they adopt the same convention, but examination of the Geodyn computer codes reveals that the factor (R_2/r) is always equivalent to the identical factor used for the static Stokes coefficients, and these are nearly always taken as (a_e/r) where a_e is the the mean equatorial radius.

The other orbit groups apparently follow Eanes *et al.* (1983)—as do the IERS conventions—by expressing the ocean tide potential as

$$U(r,\theta,\varphi,t) = \frac{GM}{r} \cdot \frac{4\pi G\rho_w}{g_e} \left(\frac{1+k_2'}{5}\right) \left(\frac{a_e}{r}\right)^2 \zeta(\theta,\varphi,t) \tag{18}$$

where M is the mass of the earth and $g_e = 9.7803\ \mathrm{m\,s^{-2}}$ is the acceleration of gravity at the equator. Comparison of (17) and (18) shows that they are equivalent only if $R_1 = GM/(g_e a_e) = 6390$ km.

A final additional complication arises from the use of a complex k_2 Love number in the GRIM5 solution. We must adjust their reported (D,ψ) estimates to ones that assume an elastic body tide, consistent with the theory worked out in Section 3 above. To do this, we construct two expressions

for the secondary potential $\hat{\Phi}^S$ as in Eq. (9), identical but for the Love number. Letting subscript 'O' denote the original tidal estimates and Love number and 'N' the new, we have

$$D_N^T e^{-i\psi_N^T} = D_O^T e^{-i\psi_O^T} + (k_O - k_N)\bar{H}\left[\alpha(1+k')\right]^{-1}. \tag{19}$$

For the GRIM5 Love number, the tidal coefficients must be incremented as follows:

$$\Delta\, D\cos\psi: \quad -0.106 \text{ cm}$$
$$\Delta\, D\sin\psi: \quad 0.136 \text{ cm}$$

Only the GRIM5 solution requires such an adjustment. The other solutions in Table 2 use the real Love number of Wahr (1981) adopted here.

The tidal coefficients (D, ψ) from all tracking solutions have been accordingly adjusted to account for the above inconsistencies in geophysical constants. That is, they have been adjusted so that the potential U is of form (17) with $\rho_w = 1035$, $k_2 = 0.302$, $k_2' = -0.307$, and $R_1 = R_2 = a$ (the mean radius). The adjusted coefficients appear in the final two columns of Table 2. Comparisons of the original and adjusted coefficients show that the adjusted ones are internally more consistent, in addition to being consistent with the theory adopted in Section 3.

As our adopted tracking solution we take the weighted mean of the six tabulated solutions. Thus, for the out-of-phase component,

$$D^T \sin\psi^T = 3.295 \sin 128.69° = 2.572 \pm 0.016 \text{ cm} \tag{20}$$

The error bar assumes the six solutions are independent (not strictly true), but it has been inflated to allow for a possible 1% error in our adopted k_2' and 0.2% error in ρ_w.

6 LUNAR ATMOSPHERIC TIDE COEFFICIENTS

The theory worked out in Section 3 allows for the effect of the lunar atmospheric tide. We require coefficients E, χ as employed in Eq. (8), similar to those in (1) but in terms of surface pressure

To our knowledge the most thorough (and still most recent) analysis and spherical harmonic decomposition of the lunar air tide is that of Haurwitz & Cowley (1969). Their decomposition was performed on global tidal charts that they constructed by subjective interpolation of 104 station values where the lunar tide had previously been estimated from long time series of barometric pressure measurements. From their analysis one finds that over 90% of the variance of the tide is accounted for by the main (2, 2) westward propagating wave (see discussion by Platzman 1991); this wave has a small phase lag of about half an hour relative to the local tidal potential. Platzman (1991) used these data (plus similar coefficients for the ocean tide) to conclude that the lunar atmospheric tide dissipates about 10 gigawatts of power.

Haurwitz and Cowley tabulated spherical harmonic coefficients corresponding to normalized Legendre functions. Converting to the unnormalized functions used here, we find

$$E = 1.84\,\mathrm{Pa}, \qquad \chi = 14.8^\circ. \tag{21}$$

These coefficients correspond to the annual mean of M_2.

7 TIDAL LAG, Q, AND DISSIPATION

The discrepancy between the altimeter and tracking solutions discussed in Sections 4 and 5 amount to 0.1 cm in the out-of-phase component $D \sin\psi$, far larger than the individual standard error estimates. Given these solutions, we are now in position to estimate the body tide lag ϵ and load tide lag ϵ' with Eq. (11). Before doing so, however, a rudimentary error analysis is needed; it will show that our satellite estimates give useful observational constraints on ϵ, but that they give no useful information at all about ϵ'.

7.1 Standard errors in phase lags

Consider Eq. (11), simplified by ignoring the atmospheric tide and the relatively small final term involving h'. Taking the real components lead to

$$\epsilon' \approx \frac{1+k'}{k'} \left(D^T \cos\psi^T - D^A \cos\psi^A \right) / (2.47\,\mathrm{cm}). \tag{22}$$

This approximation for ϵ' is equivalent to (15) for ϵ. Given the standard errors in the altimeter and tracking tide estimates, Eq. (22) implies that the standard error in the estimate of ϵ' will be roughly

$$\sigma_{\epsilon'} = 0.913 \times \sqrt{(0.015^2 + 0.016^2)} = 1.1^\circ \tag{23}$$

This error estimate is actually too conservative, because it neglects errors in the adopted h_2 and k_2 which do not affect the out-of-phase tidal estimates but could affect the in-phase ones. Nonetheless, the uncertainty 1 1° is already so large that the estimate of ϵ' can be of no geophysical interest. The lag in k' is expected to be one, possibly two, orders of magnitude smaller than this error estimate. Published model estimates of the lag in k' are, for example, 0.010° (Pagiatakis 1990) and 0 033° (Zschau 1978). Zschau (1978) finds the lag ϵ' to be significantly smaller than ϵ.

A similar analysis for ϵ gives $\sigma_\epsilon = 0.047^\circ$. This is sufficiently small that the estimate of ϵ is indeed of interest. (The large difference in these two error limits stems from the fact that ϵ' in (11) or (22) is scaled by the small tidal coefficient $D \sin\psi$, while ϵ is not.) The large error in ϵ' does imply that we must examine a wide range of values to bound its effect on estimates of ϵ.

7.2 Estimated body-tide phase lag

Solving Eq. (11) for both tidal phase lags yields the estimates: $\epsilon = 0.233°$, $\epsilon' = -1.14°$. The latter is geophysically implausible, but not unexpected given the large error limits for ϵ'. If we solve (11) for ϵ as a function of ϵ', we find $\epsilon = 0.23°$, 0 20°, 0.18°, when $\epsilon' = -1°$, 0°, +1°, respectively On geophysical grounds, and noting previous model calculations that suggest $\epsilon' \ll 1°$, one must conclude that the middle estimate is preferable. Our estimate of the body-tide lag is therefore

$$\epsilon = 0.204° \pm 0.047°$$

The error limits already cover the range of values caused by our lack of knowledge of ϵ'.

The air tide turns out to be marginally important, it causes a small 0.01° contribution to ϵ. (Being nearly in phase with the tidal potential, its contribution to ϵ' is more important.)

The body tide lag implies an effective tidal Q of 280 with 1-σ error bounds of (230, 360).

7.3 Body tide energy dissipation

The anelasticity that induces the lag ϵ in the earth's body tide implies a certain loss of tidal energy Platzman (1984) has shown that the energy dissipation rate in given by

$$P = 101.4\,\mathrm{TW} \times k_2 \sin\epsilon, \tag{24}$$

which implies

$$P = 110 \pm 25\ \mathrm{GW}.$$

For comparison this is 22 times smaller than the M_2 dissipation rate in the oceans (Cartwright & Ray 1991), but an order of magnitude greater than the rate in the atmosphere (Platzman 1991).

It is important to realize that this dissipation rate is for the body tide alone. There exists additional solid-earth tidal dissipation caused by the ocean's load deformation. This depends on the lag in k_n' for all n, and thus also depends on all spherical harmonics of the ocean tide. Platzman (1984) estimated this load-tide contribution to tidal dissipation and concluded that it is an order of magnitude smaller than the dissipation in the body tide. His results, of course, are dependent on his adopted k_n'. The results of our paper cannot contribute to this discussion; they apply only to the body tide.

7.4 Corrected oceanic coefficients

The ocean tide coefficients of Table 1 are the result of correcting T/P altimetry by an elastic model of the body tide. It is worthwhile to examine the magnitude of this error, given our estimate of ϵ, and if necessary correct these coefficients to more accurately represent the pure ocean tide The error is the term $\Delta\zeta_b$ from (10), which is

$$\Delta\zeta_b = h\bar{H}\left(e^{-i\epsilon} - 1\right) \approx -ih\bar{H}\epsilon = -i\,0.0173\,\mathrm{cm}. \tag{25}$$

The error is almost completely imaginary and amounts to about half a percent. That is, the altimeter coefficient $D\sin\psi$ should be reduced by 0.0173 cm. Therefore, a more accurate estimate of the true ocean tide may be had by replacing the altimetric esimate of Eq. (16) by

$$D\sin\psi = 3.206\sin 130.012^\circ = 2.455 \pm 0.015\,\mathrm{cm}. \tag{26}$$

Of course, a similar exercise can be done for the tracking estimates, for which the adjustment will be significantly larger But in that case, one should also correct for the air tide as well as the lagged body tide. There will thus be an adjustment to both the in-phase and out-of-phase components.

This estimate of $D\sin\psi$ for the ocean implies (Platzman 1984; Cartwright & Ray 1991) an oceanic tidal dissipation of 2.421 ± 0.015 TW. The tracking coefficients (20) imply a planetary dissipation of $2\,536 \pm 0.016$ TW. The difference of 115 GW is contributed by the solid tide and the air tide. (These estimates, based on Platzman's Eqs. (10) and (26), again assume no significant dissipation in the load tide, i e. that $\epsilon' \approx 0$.)

8 DISCUSSION

It is generally supposed that the earth's Q is weakly dependent on frequency; for example, $Q \sim \omega^\alpha$ where α is between 0.1 and 0.3 (Anderson & Minster 1979). It is conceivable that this simple form holds over a frequency range of many decades, although Ivins & Sammis (1995) investigate a more complicated frequency dependence resulting from a mixture or composite model of the mantle. The empirical data for establishing $Q(\omega)$ are not strong, so a precise estimate at the semidiurnal frequency is of some value.

Table 3 gathers together a number of model and observational estimates of the earth's semidiurnal Q. Estimates such as those of Wahr & Bergen (1986) adopt Earth models deduced primarily from seismic and free-oscillation data, along with some ω^α frequency dependence. Both tabulated Earth models in Table 3 agree well with our esimates, with the bounds given by Wahr & Bergen (1986) considerably tightened.

Three of the entries in Table 3 rely on estimates of the complex displacement Love number h_2. (We again assume that the lag in h_2 is not far from that in k_2) Of most interest are those analyses employing very long baseline interferometer (VLBI) data, which result in a direct geometrical measurement of h_2, essentially by observing the vertical tidal motions at the VLBI stations The Herring-Dong estimate implies an ϵ that is more than double ours, although with an admittedly large uncertainty. The VLBI data are sensitive to the entire solid tide, so the body tide is separated from the load tide by applying ocean-loading corrections at all stations. The degree-2 part of the load tide correction bears directly on

the accuracy on the h_2 solution, and in this regard it is important to note that Herring & Dong (1994) used the Schwiderski (1983) model, whose degree-2 term is fairly inaccurate according to our Figure 1. A simple calculation, based on the size of Schwiderski's error in Figure 1, suggests that the error in the VLBI load tide would act to inflate the estimate of the phase in h_2. The more recent VLBI analysis of Schuh & Haas (1998) used a more modern load-tide correction, and their results for ϵ are consistent with ours.

The one completely discrepant entry in Table 3 is that of Melchior (1989), who deduced a 0.38° lag in the gravity tide from an analysis of Earth tide measurements at 292 stations. Notwithstanding their inherently high precisions, gravimeter observations of tides are somewhat insensitive to a body lag—the radial deformation of the surface partly cancels the gravity effect of redistributed mass—and a lag ϵ in the secondary tidal potential materializes as a gravity lag of only $\epsilon/7.7$ (Lambeck 1988, p 579). Hence, Melchior's 0.38° lag implies $\epsilon = 3°$, or a solid-earth Q of only 20. (Zschau & Wang (1986), using a depth-dependent anelastic model, calculate that the gravity lag is an even smaller fraction of ϵ, which would imply a gravity-inferred Q even smaller than 20.) The reasons for this anomalous result are most likely calibration errors in the gravimeters (Baker *et al.* 1989) and possibly poor ocean loading corrections (the Schwiderski model was used for all stations).

9 CONCLUSIONS

By themselves neither satellite tracking data nor satellite altimeter data can distinguish an earth-tide lag from an ocean-tide lag. In combination, however, they may do so, if each is sufficiently precise. For M_2 we find the lag in the earth's body tide to be $0.204° \pm 0.047°$. This represents so far the most direct and most precise determination of the effect of the earth's anelastic dispersion at half-daily periods. It stems from marked advances in both tracking and altimeter estimates, as Figures 1 and 2 make clear. No comparably useful information about the lag in the load tide could be obtained

Eventually one expects satellite geodetic constraints on anelasticity at a number of tidal periods This has been accomplished for the 18.6-year tide, under the reasonable assumption that the ocean tide is in equilibrium with the generating potential and has no out-of-phase component (Eanes 1995). Other long-period tides await improvements in the ocean models, especially in the data-sparse polar oceans where the P_2^0 function attains its maximum (e.g., Desai & Wahr, 1999) To some extent, the far Southern Ocean is also a limiting factor for diurnal tides—they all display an intense Antarctic Kelvin wave that noticeably contributes to P_2^1, the lunar tide O_1 appears to hold the most promise for the immediate future.

ACKNOWLEDGMENTS

We thank Gary Egbert, Richard Biancale, and M.-K. Cheng for use of their unpublished tidal estimates, including error bars. David Rowlands and Richard Biancale provided invaluable help in determining the various geophysical constants used in satellite tracking analyses. R.D.R. especially thanks George W. Platzman for many extended discussions on tidal energy dissipation.

REFERENCES

Anderson, D. L. & Minster, J. B., 1979. The frequency dependence of Q and implications for mantle rheology and Chandler wobble, *Geophys. J. R. astr Soc.*, **58**, 431–440.

Baker, T. F., Edge, R. J., & Jeffries, G., 1989. European tidal gravity: an improved agreement between observations and models, *Geophys. Res. Lett.*, **16**, 1109–1112

Bogdanov, K T. & Magarik, V. A., 1967 Numerical solutions for the world's semidiurnal tides, *Dokl Akad Nauk. SSSR*, **172**, 1315–1317.

Cartwright, D E. & Ray, R D., 1991. Energetics of global ocean tides from Geosat altimetry, *J geophys Res* , **96**, 16897–16912

Cartwright, D. E. & Tayler, R. J., 1971. New computations of the tide-generating potential, *Geophys. J. R. astr Soc.*, **23**, 45–74

Cazenave, A & Daillet, S , 1981. Lunar tidal acceleration from earth satellite orbit analysis, *J. geophys Res.*, **86**, 1659–1663.

Cazenave, A , Daillet, S. & Lambeck, K , 1977 Tidal studies from perturbations in satellite orbits, *Phil. Trans R. Soc.*, **A284**, 595–606.

Cheng, M. K , Shum, C K., Eanes, R. J , Schutz, B. E. & Tapley, B. D., 1990. Long-period perturbations in Starlette orbit and tide solution, *J. geophys. Res.*, **95**, 8723–8736.

Cheng, M. K., Shum, C. K., & Tapley, B. D., 1997. Determination of long-term changes in the Earth's gravity field from satellite laser ranging observations, *J geophys. Res* , **102**, 22377–22390.

Christodoulidis, D. C., Smith, D. E , Williamson, R. G., & Klosko, S. M., 1988. Observed tidal braking in the Earth/Moon/Sun system, *J geophys. Res.*, **93**, 6216–6236.

Daillet, S , 1978. Détermination par observation des trajectoires de satellites artificiels des ondes semi-diurnes de la marée océanique, *Ann. Geophys* , **34**, 79–87.

Desai, S. D & Wahr, J. M , 1999. Monthly and fortnightly tidal variations of the earth's rotation rate predicted by a Topex/Poseidon empirical ocean tide model, *Geophys. Res Lett.*, **26**, 1035–1038.

Dushaw, B D., Egbert, G. D., Worcester, P. F , Cornuelle, B. D , Howe, B M., & Metzger, K , 1997 A Topex/Poseidon global ocean tidal model and barotropic tidal currents determined from long-range acoustic transmissions, *Prog. Oceanog.*, **40**, 337–367

Eanes, R J , 1995 A study of temporal variations in Earth's gravitational field using Lageos-1 laser range observations, CSR-95-8, University of Texas, Austin, 128 pp.

Eanes, R. J., Schutz, B., & Tapley, B , 1983 Earth and ocean tide effects on Lageos and Starlette, in *Proceedings of the Ninth Int. Symposium on Earth Tides*, (Ed.. J. T. Kuo), Schweizerbart'sche Verlagsbuchhandlung, Stuttgart, pp. 239–249

Egbert, G. D., Bennett, A F., & Foreman, M. G G , 1994 Topex/Poseidon tides estimated using a global inverse model, *J geophys Res.*, **99**, 24821–24852.

Farrell, W E , 1972 Deformation of the earth by surface loads, *Rev Geophys. Space Phys* , **10**, 761–797

Gendt, G & Dietrich, R., 1988 Determination of geodynamical parameters based on Lageos laser ranging data, *Gerlands Beitr Geophys* , **97**, 438–449.

Gill, A., 1982 *Atmosphere-Ocean Dynamics*, Academic Press, Orlando.

Goad, C. C. & Douglas, B. C , 1978. Lunar tidal acceleration obtained from satellite-derived ocean tide parameters, *J. geophys. Res* , **83**, 2306–2310.

Han, D., & Wahr, J., 1995. The viscoelastic relaxation of a realistically stratified Earth and a further analysis of post-glacial rebound, *Geophys J Int.*, **120**, 287–311.

Harwood, N. M. & Swinerd, G. G., 1997. Ocean-tide parameters from the simultaneous long-period analysis of the orbits of Starlette and Stella, *Ann. Geophysicae*, **15**, 263–271

Haurwitz, B , & Cowley, A D., 1969 The lunar barometric tide, its global distribution and annual variation, *Pure Appl. Geophys* ,**77**, 122–150.

Hendershott, M C , 1972 The effects of solid earth deformation on global ocean tides, *Geophys. J. R. astr Soc.*, **29**, 389–402

Herring, T A. & Dong, D , 1994 Measurement of diurnal and semidiurnal rotational variations and tidal parameters of the Earth, *J geophys Res* , *99*, 18051–18071.

Ivins, E. R & Sammis, C G , 1995. On lateral viscosity contrast in the mantle and the rheology of low-frequency geodynamics, *Geophys. J Int* , **123**, 305–322.

Kozai, Y , 1968. Love's number of the earth derived from satellite observations, *Publ. Astron. Soc. Japan*, **20**, 24–26.

Lambeck, K., 1977. Tidal dissipation in the oceans: astronomical, geophysical, and oceanographic consequences, *Phil Trans. R. Soc.*, **A287**, 545–594.

Lambeck, K., 1988. *Geophysical Geodesy*, Clarendon Press, Oxford

Lambeck, K , Cazenave, A. & Balmino, G , 1974. Solid earth and ocean tides estimated from satellite orbit analyses, *Rev. Geophys Space Phys.*, **12**, 421–434.

Lemoine, F G., Kenyon, S. C , Factor, J. K., Trimmer, R. G , Pavlis, N K , Chinn, D. S., Cox, C. M , Klosko, S. M , Luthcke, S. B , Torrence, M H., Wang, Y. M., Williamson, R G , Pavlis, E. C., Rapp, R H., & Olsen, T. R., 1998. The development of the joint NASA GSFC and NIMA geopotential model EGM96, *NASA Tech. Memo 206861*, Goddard Space Flight Center, Greenbelt, 575 pp

Le Provost, C., Genco, M. L., Lyard, F , Vincent, P , & Canceil, P., 1994 Tidal spectroscopy of the world ocean tides from a finite element hydrodynamic model, *J. geophys Res* , **99**, 24777–24798

Le Provost, C., Lyard, F., Molines, J.-M., Genco, M. L., & Rabilloud, F, 1998. A hydrodynamic ocean tide model improved by assimilating a satellite altimeter-derived data set, *J. geophys Res* , **103**, 5513–5529.

Lerch, F. J. *et al.*, 1992 Geopotential models of the Earth from satellite tracking, altimeter, and surface gravity observations: GEM-T3 and GEM-T3S, *NASA Tech. Memo. 104555*, Goddard Space Flight Center, Greenbelt, 128 pp

Marsh, J. G. *et al.*, 1990 The GEM-T2 gravitational model, *J. geophys. Res* , **95**, 22043–22071.

McCarthy, D. (editor), 1996 IERS Conventions, IERS Tech Note 21, International Earth Rotation Service, Observatoire de Paris, 95 pp

Melchior, P, 1989. The phase lag of Earth tides and braking of the Earth's rotation, *Phys. Earth Planet. Inter.*, **56**, 186–188

Moore, P, 1987. Ocean tidal parameters from Starlette data, *Bull Géod.*, **61**, 223–234.

Newton, R. R., 1968. A satellite determination of tidal parameters and earth deceleration, *Geophys. J. R. astr. Soc* , **14**, 505–539.

Pagiatakis, S. D., 1990 The response of a realistic earth to ocean tide loading, *Geophys. J Int.*, **103**, 541–560

Parke, M E & Hendershott, M C., 1980. M2, S2, K1 models of the global ocean tide on an elastic earth, *Marine Geod.*, **3**, 379–408

Pekeris, C. L. & Accad, Y., 1969. Solution of Laplace's equations for the M_2 tide in the world oceans, *Phil. Trans. R. Soc.* A, **265**, 413–436.

Platzman, G. W., 1984. Planetary energy balance for tidal dissipation, *Rev. Geophys. Space Phys.*, **22**, 73–84.

Platzman, G W., 1991 An observational study of energy balance in the atmospheric lunar tide, *Pure Appl. Geophys.*,**137**, 1–33

Ray, R. D., 1999. A global ocean tide model from Topex/Poseidon altimetry: GOT99 2, *NASA Tech. Memo. 209478*, Goddard Space Flight Center, Greenbelt, 58 pp.

Ray, R. D , Bettadpur, S., Eanes, R. J , & Schrama, E J. O., 1995. Geometrical determination of the Love number h_2 at four tidal frequencies, *Geophys. Res. Lett.*, **22**, 2175–2178.

Ray, R. D , Eanes, R. J. & Chao, B. F., 1996 Detection of tidal dissipation in the solid Earth by satellite tracking and altimetry, *Nature*, **381**, 595–597.

Schuh, H & Haas, R., 1998. Earth tides in VLBI observations, in *Proceedings of the 13th Intl Symposium on Earth Tides*, eds.. B Ducarme & P Pâquet, Observ Royal Belgique, Brussels, pp. 101–110.

Schrama, E. J. O. & Ray, R. D., 1994. A preliminary tidal analysis of Topex/Poseidon altimetry, *J. geophys. Res* , **99**, 24799–24808.

Schwiderski, E W, 1983. Atlas of ocean tidal charts and maps: I. The semdiurnal principal lunar tide M_2, *Marine Geod.*, **6**, 219–265.

Schwintzer, P., Reigber, C , Massmann, F-H., Barth, W , Raimondo, J. C., Gerstl, M., Li, H., Biancale, R , Balmino, G , Moynot, B., Lemoine, J. M., Marty, J. C , Boudon, Y. & Barlier, F., 1991. A new earth gravity field model in support of ERS-1 and SPOT-2: GRIM4-S1/C1, DARA/CNES, Munchen/Toulouse, 177 pp

Schwintzer, P. *et al* , 1997. Long-wavelength global gravity field models: GRIM4-S4, GRIM4-C4, *J. Geod.*, **71**, 189–208

Schwintzer, P. *et al.*, 1999 Development of GRIM5 Earth's gravitational models (abstract), *Eos*, **80**, Fall Meeting Suppl , p. F254.

Shum, C. K. *et al* , 1997. Accuracy assessment of recent ocean tide models, *J. geophys Res.*, **102**, 25173–25194

Smith, D. E., Kolenkiewicz, R & Dunn, P J 1973 Earth tidal amplitude and phase, *Nature*, **244**, 498–499.

Wahr, J. M., 1981. Body tides on an elliptical, rotating, elastic and oceanless earth, *Geophys J. R. astr Soc.*, **64**, 677–703.

Wahr, J. M & Bergen, Z , 1986. The effects of mantle anelasticity on nutations, earth tides, and tidal variations in rotation rate, *Geophys. J. R. astr Soc* , **87**, 633–668

Williamson, R. G. & Marsh, J G., 1985 Starlette geodynamics: the earth's tidal response, *J. geophys. Res.*, **90**, 9346–9352.

Wunsch, C. & Stammer, D., 1995. The global frequency-wavenumber spectrum of oceanic variability from Topex/Poseidon altimetric measurements, *J geophys. Res.*, **100**, 24895–24910.

Zahel, W , 1970. Die Reproduktion gezeitenbedingter Bewegungsvorgange im Weltozean mittels des hydrodynamisch-numerischen Verfahrens, *Mitt Inst. f Meerkd Hamburg*, **17**, 1–50

Zahel, W., 1977. A global hydrodynamic-numerical 1°-model of the ocean tides, *Ann. Geophys.*, **33**, 31–40.

Zschau, J., 1978. Tidal friction in the solid earth: loading tides versus body tides, in *Tidal Friction and the Earth's Rotation*, eds : P Brosche & J. Sundermann, Springer-Verlag, Berlin, pp. 62–94.

Zschau, J., 1986. Tidal friction in the solid earth: constraints from the Chandler Wobble period, in *Space Geodesy and Geodynamics*, eds.: A. Anderson & A Cazenave, Academic Press, London, pp. 315–344.

Zschau, J & Wang, R., 1986. Imperfect elasticity in the earth's mantle: implications for earth tides and long period deformations, in *Proceedings of the Tenth Intl. Symposium on Earth Tides*, ed.: R Vieira, Consejo Superior de Invest. Cientificas, Madrid, pp 379–384.

This paper has been produced using the Blackwell Scientific Publications GJI LaTeX2e class file.

Table 1. M_2 spherical harmonic components from altimetry

Author	Solution	D_{22}^+, cm	ψ_{22}^+	σ,cm
Ray, 1999	GOT99.2	3.230	129.97°	–
Egbert	TPXO.4a	3.223	129.99°	0.013
Eanes	CSR4.0	3.229	129 41°	–
Le Provost et al., 1998	FES95.2	3.193	129 89°	–

Table 2. M_2 ocean tide coefficients from satellite tracking analyses

		Reported						Adjusted	
Author	Solution	D_{22}^+, cm	ψ_{22}^+	σ, cm	ρ_w	$-k_2'$	k_2	$D\sin\psi$	$-D\cos\psi$
Lerch et al., 1992	GEM-T3S	3.31	128.9°	0.04	1031	0.310	0.302	2.563	2.069
Eanes	LLA96-1	3.322	128.8°	0.03	1025	0.3075	0.302	2.578	2.073
Eanes	LLA96-2	3 292	128.8°	0 04	1025	0 3075	0 302	2.555	2 054
Cheng	7/97	3.33	128.8°	0.02	1025	0.3075	0.302	2.583	2.076
Lemoine et al., 1998	EGM96S	3.266	128.2°	0.024	1031	0.310	0.302	2.554	2.010
Schwintzer et al.,1999	GRIM5-S1	3.193	128 9°	0.018	1025	0.3142	.301−*i*.0013	2.580	2.077

Tabulated entries for Love numbers and seawater density are those used in original solutions. "Adjusted" coefficients correspond to solutions with $k_2 = 0.302$, $k_2' = -0.307$, $\rho_w = 1035\ \mathrm{kg\,m^{-3}}$.

Table 3. Estimates of earth's Q at semidiurnal period

Authors	Method	Love number	ϵ	Q	
Wahr & Bergen, 1986	Earth model QMU	$k_2 = 0.3050 - i.0013$	0.24°	235	
	lower bound	$0.3040 - i.0006$	0 11°	507	
	upper bound	$0.3170 - i.0036$	0 65°	88	
Buffett & Mathews*	Earth model	$k_2 = 0\ 3010 - i.0013$	0 25°	230	
Herring & Dong, 1994	VLBI	$h_2 = .604 - i.005 \pm 002$	0 47° ± 0.20°	120	(85,210)
Schuh & Haas, 1998	VLBI	$h_2 = .600 - i.003 \pm .001$	0.29° ± 0.10°	200	(150,300)
Ray et al., 1995	Topex + tide gauges	$h_2 = 613 - i.000 \pm .007$	0.00° ± 0.65°		
Zschau, 1986	Chandler wobble		0.21°	270	
	lower bound		0 14°	420	
	upper bound		0 26°	220	
Melchior, 1989	Gravimetry 0 38°lag		2.9°	20	
This paper	Satellites		0.20° ± 0.05°	280	(230,360)

* Quoted in McCarthy (1996).

Figure 1. Historical snapshots of our knowledge of the $D_{22}^{+}, \psi_{22}^{+}$ coefficients of the M_2 ocean tide. Open circles represent estimates from sátellite tracking data. Filled circles represent estimates from either hydrodynamic models or satelllite altimeter data. Labels refer to the following authors (note that some tidal parameters are extracted from Lambeck (1977) and may not appear in the original citation):

(a) B-M (Bogdanov & Magarik 1967), C (Cazenave et al. 1977), E (Estes 1977), H (Hendershott 1972), P-A (Pekeris & Accad 1969) Z (Zahel 1970, 1977).

(b) C-D (Cazenave & Daillet 1981), D (Daillet 1978), G-D (Goad & Douglas 1978), M (Moore 1987), P-H (Parke & Hendershott 1982), S (Schwiderski 1983), W-M (Williamson & Marsh 1985).

(c) C (Cheng *et al.* 1990), C-R (Cartwright & Ray 1991), G-D (Gendt & Dietrich 1988), G4 (Schwintzer *et al.* 1991), P-H (Parke & Hendershott 1982), S (Schwiderski 1983), T1 (Christodoulidis *et al.* 1988), T2 (Marsh *et al* 1990).

(d) E (Eanes, unpublished), R (Ray, unpublished), S-R (Schrama & Ray 1994, updated), T3 (Lerch *et al* 1992).

Figure 2. Estimates of the M_2 ocean tide (2,2) coefficients from satellite tracking data (open circles) and T/P altmeter data (closed circles) The data are extracted from Tables 1 and 2 The tracking estimates have been adjusted for consistency as described in Section 5.1. Both data types are based on strictly elastic models of the solid tide

Figure 1. Historical snapshots of our knowledge of the $D_{22}^{+}, \psi_{22}^{+}$ coefficients of the M_2 ocean tide Open circles represent estimates from satellite tracking data. Filled circles represent estimates from either hydrodynamic models or satellite altimeter data. Labels refer to the following authors (note that some tidal parameters are extracted from Lambeck (1977) and may not appear in the original citation)
(a) B-M (Bogdanov & Magarik 1967), C (Cazenave et al 1977), E (Estes 1977), H (Hendershott 1972), P-A (Pekeris & Accad 1969) Z (Zahel 1970, 1977)
(b) C-D (Cazenave & Daillet 1981), D (Daillet 1978), G-D (Goad & Douglas 1978), M (Moore 1987), P-H (Parke & Hendershott 1982), S (Schwiderski 1983), W-M (Williamson & Marsh 1985)
(c) C (Cheng *et al* 1990), C-R (Cartwright & Ray 1991), G-D (Gendt & Dietrich 1988), G4 (Schwintzer *et al* 1991), P-H (Parke & Hendershott 1982), S (Schwiderski 1983), T1 (Christodoulidis *et al* 1988), T2 (Marsh *et al.* 1990)
(d) E (Eanes, unpublished), R (Ray, unpublished), S-R (Schrama & Ray 1994, updated), T3 (Lerch *et al* 1992)

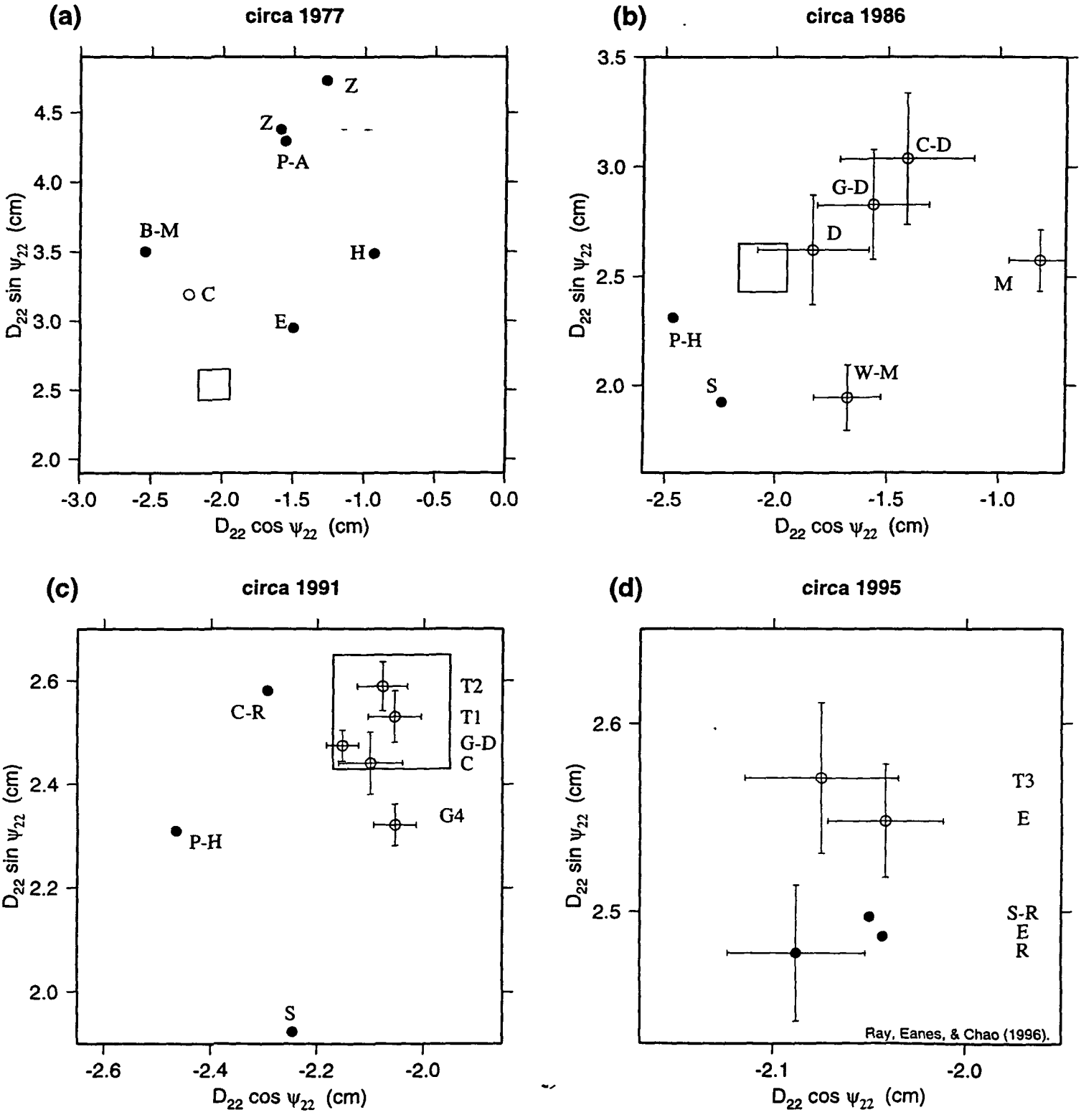

Figure 2. Estimates of the M_2 ocean tide (2,2) coefficients from satellite tracking data (open circles) and T/P altimeter data (closed circles). The data are extracted from Tables 1 and 2. The tracking estimates have been adjusted for consistency as described in Section 5.1. Both data types are based on strictly elastic models of the solid tide.